


## Article

# Impact of Rock Cuttings on Downhole Fluid Movement in Polycrystalline Diamond Compact (PDC) Bits, Computational Fluid Dynamics, Simulation, and Optimization of Hydraulic Structures

Lihong Wei <sup>1,2,\*</sup> and Jaime Honra <sup>1</sup> 

<sup>1</sup> School of Mechanical, Manufacturing and Energy Engineering, Mapúa University, Manila 1002, Philippines; jphonra@mapua.edu.ph

<sup>2</sup> School of Intelligent Manufacturing, Leshan Vocational and Technical College, Leshan 614000, China

\* Correspondence: lnwei@mymail.mapua.edu.ph; Tel.: +86-13096317506

**Abstract:** The flow occurring at the bottom of a polycrystalline diamond compact (PDC) drill bit involves a complex process made up of drilling fluid and the drilled rock cuttings. A thorough understanding of the bottom-hole flow conditions is essential for accurately evaluating and optimizing the hydraulic structure design of the PDC drill bit. Based on a comprehensive understanding of the hydraulic structure and fluid flow characteristics of PDC drill bits, this study integrates computational fluid dynamics (CFD) with rock-breaking simulation methods to refine and enhance the numerical simulation approach for the liquid–solid two-phase flow field of PDC drill bits. This study further conducts a comparative analysis of simulation results between single-phase and liquid–solid two-phase flows, highlighting the influence of rock cuttings on flow dynamics. The results reveal substantial differences in flow behavior between single-phase and two-phase conditions, with rock cuttings altering the velocity distribution, flow patterns, and hydraulic performance near the bottom-hole region of the drill bit. The two-phase flow simulation results demonstrate higher accuracy and provide a more detailed depiction of the bottom-hole flow, facilitating the identification of previously unrecognized issues in the hydraulic structure design. These findings advance the methodology for multiphase flow simulation in PDC drill bit studies, providing significant academic and engineering value by offering actionable insights for optimizing hydraulic structures and extending bit life.

**Keywords:** PDC drill bit; CFD; liquid–solid two-phase flow; hydraulic structure



Academic Editors: Beatrice Pulvirenti and Jun Yao

Received: 23 September 2024

Revised: 28 November 2024

Accepted: 11 December 2024

Published: 14 January 2025

**Citation:** Wei, L.; Honra, J. Impact of Rock Cuttings on Downhole Fluid Movement in Polycrystalline Diamond Compact (PDC) Bits, Computational Fluid Dynamics, Simulation, and Optimization of Hydraulic Structures. *Fluids* **2025**, *10*, 13. <https://doi.org/10.3390/fluids10010013>

**Copyright:** © 2025 by the authors. Licensee MDPI, Basel, Switzerland. This article is an open access article distributed under the terms and conditions of the Creative Commons Attribution (CC BY) license (<https://creativecommons.org/licenses/by/4.0/>).

## 1. Introduction

Drilling is a crucial process in oil resource development, with drill bits serving as critical tools for rock fragmentation. The performance of these drill bits directly impacts the cost, efficiency, and quality of drilling operations. In recent years, with the introduction of PDC bits and advancements in drilling technology, PDC bits have become highly efficient, economical, and safe tools for rapid drilling [1–3]. As oil-drilling trends shift towards offshore and deeper wells, the design requirements for PDC bits have also become more stringent. The design of PDC bits includes the structure of the cutters and the hydraulic structure. The design and manufacturing processes of the cutters directly influence the performance of the PDC bits, while the hydraulic structure design plays a critical role throughout the drilling process [4–6]. The hydraulic structure refers primarily to the design of flow channels and nozzles on the bit, which control the flow path, velocity, and pressure

distribution of the drilling fluid, thereby impacting the cooling and cleaning efficiency of the bit. During the rock-breaking drilling process, PDC bits generate numerous cuttings. If these cuttings are not promptly removed, they can accumulate at the bottom of the well, leading to poor hole cleaning and posing a significant risk to well safety, potentially resulting in complications, such as wellbore blockages or blowouts. In severe cases, the accumulation of rock cuttings may result in bit-balling—mud-like clumps composed of cuttings, drilling fluid, and fine formation particles that accumulate on the bit surface [7,8]. Additionally, frictional heat generated during drilling raises the temperature of the cutters surfaces. If the rock cuttings are not efficiently cleared, this can hinder the convective cooling effect of the drilling fluid on the bit, leading to inadequate cooling and potential thermal wear failure, ultimately affecting the lifespan and drilling efficiency of the bit [9,10]. Saifulizan [11] emphasizes the importance of well safety in oil and gas drilling, focusing on conventional methods like wellbore monitoring and fluid circulation to prevent formation fluid infiltration. The research highlighted the importance of maintaining pressure above formation pressure. It also discussed hard and soft shut-in procedures for managing kicks or blowouts. It emphasized the role of automated drilling and real-time monitoring systems in improving safety and drilling efficiency. Therefore, it is crucial to prioritize well safety to prevent any hole problems like poor hole cleaning. Ensuring well safety involves designing the hydraulic structure of the PDC drill bit to improve the cooling and transportation of rock cuttings, which helps prevent hole problems and maintain efficient drilling operations.

Analyzing the bottom-hole flow can identify issues in the hydraulic structure design of drill bits, enabling adjustments to improve the rock cuttings transportation and cooling efficiency of the bits [12,13]. Scholars generally use numerical simulation methods to study the bottom hole flow of PDC drill bits. Numerical simulation offers insights into fluid flow behavior and reveals specific issues with the hydraulic structure of the bit, which enables more precise improvements in nozzle configuration and the design of flow channels, optimizing the hydraulic structure. Numerous researchers have conducted numerical simulations of the bottom-hole flow of PDC bits, making significant advancements. Hou Chen, Chen Xiuping et al. [14–17] performed numerical analyses to examine the velocity and well pressure within the flow in the bottom hole, indicating that the lateral diffusion caused by jet nozzles is the primary driving force for removing rock cuttings. Additionally, Chen Xiuping suggested that mitigating or preventing bit-balling could be achieved by enhancing drilling mud properties and adjusting drilling parameters. Rahman [18] emphasizes the importance of controlling mud density to avoid formation fractures, adjusting the yield point to improve cuttings transport, and optimizing gel strength to prevent cuttings buildup and reduce the risk of a stuck pipe, making it essential to evaluate the properties of the drilling mud to increase the efficacy of coiled tubing operations and prevent any hole problems. Kuilin Huang [19] proposed an annular-grooved PDC bit and optimized hydraulic design using numerical simulations, demonstrating an effective reduction in bit-balling failures and significant enhancement in drilling efficiency. Pengju Qu [20] studied the distribution patterns of the bottom-hole flow in PDC bits, finding that an increase in bit rotational speed and fluid velocity effectively enhances turbulent kinetic energy and velocity at the bottom of the well, which promotes cuttings migration and inhibits bit-balling formation. Wang et al. [21,22] conducted numerical simulations of bottom-hole flow in PDC drill bits at both static (non-rotating) and varying rotational speeds. Results revealed that the choice of simulation method for the rotating flow significantly influences flow distribution and variation around the PDC bits, underscoring the importance of accurately selecting and applying simulation techniques to analyze bottom-hole flow dynamics and optimize PDC drill bit performance. Chaochao Feng, Jian Zhao et al. [23–25] conducted numerical simulations to investigate critical factors influencing the erosion resistance of PDC drill bits, followed

by hydraulic design optimization, revealing that mass flow rate significantly affects the average erosion rate. Chen [26] developed a liquid–solid two-phase flow model for the bottom hole of PDC drill bits, demonstrating that increasing the nozzle angle and balancing the flow passage velocity enhance rock cuttings cleaning efficiency. Cao [27] performed numerical simulations of the two-phase flow for the enclosed coring bit, analyzing flow characteristics at the bit lip and their effects on sealing effectiveness, drilling efficiency, and service life. Jing Li [28] utilized the discrete phase model (DPM) to analyze the bottom-hole flow of PDC bits, finding that the offset blade horizontal nozzle significantly enhances the flow velocity near the PDC cutters, reduces rock cuttings concentration, and minimizes the vortex area, thereby optimizing the hydraulic performance of the drill bit.

Although significant research has been conducted on the bottom-hole flow characteristics of PDC bits, most studies have yet to consider the impact of cuttings on the flow, often simplifying it as a single-phase flow, which may result in incomplete or inaccurate simulation outcomes. Although Jing Li [28] has conducted a numerical simulation of the liquid–solid two-phase flow in the bottom-hole flow of the PDC drill bit, the initial generation position of the rock cuttings is ignored in the analysis, just assuming rock cuttings are generated directly at the bottom-hole, which does not reflect actual drilling conditions. In actual drilling conditions, rock cuttings are generated at the contact points between the PDC cutters and the formation, each with initial directions, velocities, and mass flow rates. Therefore, when performing numerical simulations, the initial location of rock cuttings generation should be set at the PDC cutter surface. Before establishing the numerical model, it is necessary to obtain the rock cuttings generation parameters for each PDC cutter and input these parameters as boundary conditions in the simulation in order to obtain more accurate simulation results that better align with the actual drilling conditions.

The main objective of the present study is to develop a more accurate numerical model for analyzing the bottom-hole flow dynamics of PDC drill bits by incorporating the effects of rock cuttings through liquid–solid two-phase flow simulations. This study aims to enhance understanding of the complex interactions between drilling fluid and cuttings. This paper hypothesizes that liquid–solid two-phase flow simulations provide a more precise and insightful bottom-hole flow analysis than a single-phase flow. While both exhibit certain similarities, the two-phase flow reveals additional distinctions and finer details crucial for understanding drilling performance. Simulations of two-phase flow are expected to yield more comprehensive research outcomes, improving the understanding of bottom-hole flow dynamics and enhancing the accuracy of optimization designs. Rock-breaking simulations are conducted to verify this hypothesis and determine initial mass flow rate, velocity, and direction of rock cuttings. The Euler–Lagrange multiphase flow model is used to describe the motion and distribution of the cuttings within the drilling fluid. This approach enables the development of a numerical model that more accurately reflects the liquid–solid two-phase flow in actual drilling conditions. By comparing the simulation results of both single-phase and two-phase flows, this study investigates the influence of rock cuttings on bottom-hole flow and assesses the advantages of the two-phase flow model in capturing key flow details.

The research results will contribute to the advancement of drilling technology, facilitating the efficient development of energy resources while providing a solid theoretical foundation and technical support for further innovations in drilling methods. By optimizing drill bit designs and improving the accuracy of numerical simulations, this study can enhance drilling efficiency, reduce energy consumption, and lower emissions, supporting the sustainable development of energy resources.

## 2. Methods

### 2.1. Theoretical Basis of Numerical Model

When performing numerical simulations of the bottom-hole flow for PDC drill bits, a thorough understanding of CFD and multiphase flow model theory is crucial for establishing a simulation model resembling actual operating conditions. During the drilling process, the solid cuttings generated by the PDC drill bit mix with the drilling fluid to form a complex multiphase flow. In this paper, the bottom-hole flow is modeled as either a single-phase flow or a liquid–solid two-phase flow, based on whether the influence of rock cuttings is included. Numerical simulations are conducted using ANSYS-CFX version 2022.R1. In the single-phase flow model, the drilling fluid is treated as a homogeneous liquid, with the fluid behavior described by the mass, momentum, and energy equations combined with a turbulence model. When considering cutting particles, the bottom-hole flow is treated as a liquid–solid two-phase flow, requiring an appropriate multiphase flow model. ANSYS-CFX version 2022.R1 offers two primary multiphase flow models: the Euler–Euler and Euler–Lagrange models [29].

The Euler–Euler model is suitable for fluids with high concentrations of dispersed phases. Each phase is treated as a continuous medium and governed by a set of independent fluid equations, with the distribution of each phase represented by its respective volume fraction. The Euler–Lagrange model is appropriate for cases with lower discrete phase concentrations, where the continuous phase is simulated using the Euler method, and the discrete phase is tracked using Lagrangian particle tracking. Since rock cuttings occupy a relatively small volume in the flow, the Lagrangian particle-tracking model is suitable for simulating the movement of rock cuttings. The Euler–Lagrange model accurately tracks the trajectory of each discrete particle. Therefore, the Euler–Lagrange model is chosen to simulate the liquid–solid two-phase flow to accurately track the trajectory of each discrete particle.

### 2.2. Basic Governing Equations of Fluids

#### 2.2.1. Single-Phase Flow Model

##### 1. Mass Conservation Equation (Continuity Equation)

Mass conservation states that the amount of fluid entering a control volume equals the amount of fluid leaving the control volume plus any changes in the amount of fluid within the control volume [30].

$$\frac{\partial \rho}{\partial t} + \nabla \cdot (\rho u) = 0 \quad (1)$$

where  $\rho$  is the drilling fluid density;  $u$  is velocity vector.

##### 2. Momentum Conservation Equation

The change in momentum of a fluid element is equal to the sum of the external forces acting on the element, such as pressure and viscous forces [30].

$$\rho \left( \frac{\partial u}{\partial t} + u \cdot \nabla u \right) = -\nabla p + \mu \nabla^2 u + f \quad (2)$$

where  $P$  is pressure;  $\mu$  is dynamic viscosity;  $f$  is body forces (such as gravity).

##### 3. Energy Conservation Equation

The change in internal energy of a fluid element is equal to the sum of the heat transferred into the element through conduction, the heat generated within the element, and the work conducted on the element by the surrounding fluid [30].

$$\rho \left( \frac{\partial e}{\partial t} + u \cdot \nabla e \right) = -\nabla \cdot q + \Phi \quad (3)$$

where  $e$  is internal energy;  $q$  is heat flux;  $\Phi$  is internal power (power loss within the fluid due to factors such as friction and turbulence).

#### 4. Turbulence Model

This paper assumes that the flow within the model is fully turbulent and employs the standard  $k$ - $\varepsilon$  model for the simulation of solutions [28,30].

$$\frac{\partial(\rho k)}{\partial t} + \frac{\partial(\rho k u_j)}{\partial x_j} = \frac{\partial}{\partial x_j} \left[ \left( \mu + \frac{\mu_t}{\sigma_k} \right) \frac{\partial k}{\partial x_j} \right] + P_k - \rho \varepsilon \quad (4)$$

$$\frac{\partial(\rho \varepsilon)}{\partial t} + \frac{\partial(\rho \varepsilon u_j)}{\partial x_j} = \frac{\partial}{\partial x_j} \left[ \left( \mu + \frac{\mu_t}{\sigma_\varepsilon} \right) \frac{\partial \varepsilon}{\partial x_j} \right] + C_1 \frac{\varepsilon}{k} P_k - C_2 \rho \frac{\varepsilon^2}{k} \quad (5)$$

where  $\mu_t$  is the turbulent viscosity;  $k$  is turbulent kinetic energy;  $\varepsilon$  is turbulent dissipation rate;  $\sigma_k$  is turbulent kinetic energy Prandtl constant;  $\sigma_\varepsilon$  is dissipation rate Prandtl constant;  $P_k$  is turbulent kinetic energy caused by viscous forces;  $C_1$  is turbulent kinetic energy dissipation rate constant;  $C_2$  is turbulent kinetic energy dissipation rate constant.

#### 5. Wall Function Model

The standard  $k$ - $\varepsilon$  model is suitable for simulating turbulent flows with high Reynolds numbers, particularly in the core region, which refers to the flow area distant from the wall boundary, where turbulence is fully developed and viscous effects are negligible. In this region, the energy cascade is dominated by inertial forces. However, the standard  $k$ - $\varepsilon$  model has limitations when applied to low-Reynolds-number turbulent flows, particularly near the wall. In these regions, turbulence is less developed due to weaker inertial forces and more vital viscous forces, resulting in a transitional state between laminar and turbulent flow. Wall functions, which are based on empirical formulas derived from experimental data, address this limitation by describing the velocity distribution and other turbulent characteristics near the wall and connecting the physical quantities at the wall to those in the core turbulent region, enhancing the performance of the model in low-Reynolds-number turbulence. The wall function model improves simulation efficiency by allowing a coarser mesh to be used near the wall, avoiding the need to refine the boundary layer mesh. The Equation is as follows [31]:

$$u^+ = \frac{1}{k} \ln(y^+) + B \quad (6)$$

where  $u^+$  is a dimensionless parameter representing the velocity;  $y^+$  is a dimensionless parameter representing the distance;  $k$  is Karman constant;  $B$  is the logarithmic law constant.

##### 2.2.2. Two-Phase Flow Model

In the two-phase flow model, the mixed flow of drilling fluid and cuttings is considered, and the liquid phase and solid phase are treated using the Euler and Lagrangian models, respectively. The governing equations of the liquid phase are the same as those of the single-phase flow model, but the motion of the solid phase is calculated using the Lagrangian particle-tracking method. During the drilling process of the drill bit, the solid particles and the drilling fluid are subjected to various external loads in the flow due to the relative speed and displacement between the liquid and solid phases. In general, the density of the cuttings is greater than the density of the drilling fluid, so the virtual mass force, pressure gradient force, and Basset force on the cuttings particles can be ignored [28,32].

## 1. Particle Force Balance Equation

$$m_p \frac{du_p}{dt} = F_p \quad (7)$$

where  $m_p$  is the mass of the particle;  $u_p$  is the velocity of the particle;  $F_p$  is the total force acting on the particle, including the drag force, buoyancy due to gravity, and rotational force.

## 2. Particle Erosion Model

Erosion damage to PDC cutters can occur due to repeated impacts from rock cuttings carried by high-velocity drilling fluid. Bit damage is primarily caused by erosion, which can significantly affect the performance and lifespan of the drill bit. The degree of erosion is related to the material properties of the PDC bit and the impact angle and velocity of the rock cuttings. To simulate the erosion of the drill bit, the Finnie erosion model is employed, and the Equation is as follows:

$$E = \left( \frac{V_P}{V_0} \right)^n f(\gamma) \quad (8)$$

$$\begin{aligned} f(\gamma) &= \frac{1}{3} \cos^2 \gamma & \tan \gamma > \frac{1}{3} \\ f(\gamma) &= \sin(2\gamma) - 3 \sin^2 \gamma & \tan \gamma \leq \frac{1}{3} \end{aligned} \quad (9)$$

where  $E$  is the erosion rate;  $V_P$  is the particle impact velocity;  $f(\gamma)$  is a dimensionless function related to the impact angle.

The impact angle is close to the arc between the particle tracking and the wall, and the general parameter value is  $n = 2.35$ ,  $V_0 = 590$  m/s.

### 2.3. Geometric Model and Meshing

#### 2.3.1. Geometric Model

This paper presents a three-dimensional model of a six-blade PDC drill bit. The modeling process defines the drill bit geometry, including blades, flow channels, and cutters, while simplifying the original model by removing insignificant features and retaining key components such as cutters and nozzles. The blades, which are crucial components responsible for rock cutting, directly affect the performance and stability of bit. The drill bit includes six blades, each equipped with PDC cutters. Each PDC cutter is numbered to describe its position and performance accurately in the simulation. The numbering follows a sequence from the center to outer edge. In addition, the flow channels need to be numbered, primarily referring to the external flow channels, which are located between the two blades and serve to discharge drilling fluid for clearing rock cuttings and cooling the drill bit. The numbering of the flow in the jet nozzles correspond to blade numbering. For example, channel 1 primarily transports cuttings generated by blade 1. A 3D model of a six-blade PDC drill bit is shown in Figure 1.

A three-dimensional bottom-hole flow model is established based on the PDC drill bit model. First, a cylindrical wellbore model is constructed using the external contour of the PDC drill bit as a reference. Based on actual drilling conditions, it is assumed that the cutting depth of the PDC cutter inserts is 3 mm, which refers to the vertical distance each cutter advances into the rock formation during one revolution of the drill bit. The inner diameter of wellbore is slightly larger than the outer diameter of drill bit to ensure proper fit. The wellbore model is combined with the drill bit model, and a Boolean subtraction operation is applied to remove the portion occupied by the drill bit, resulting in a bottom-hole flow model that accurately reflects the shape and position of drill bit.

Additionally, the boundaries required for subsequent mesh generation and numerical simulation must be defined, including naming the inlet, outlet, and wall. As shown in Figure 2, the red arrow is labeled as an inlet, where drilling fluid enters and flows into the nozzles of the drill bit. The green arrows are labeled as outlets, indicating where the drilling



fluid and rock cuttings flow out. Six outlets are individually named to correspond to six flow nozzles. The external surface of the wellbore is designated as the wall boundary.

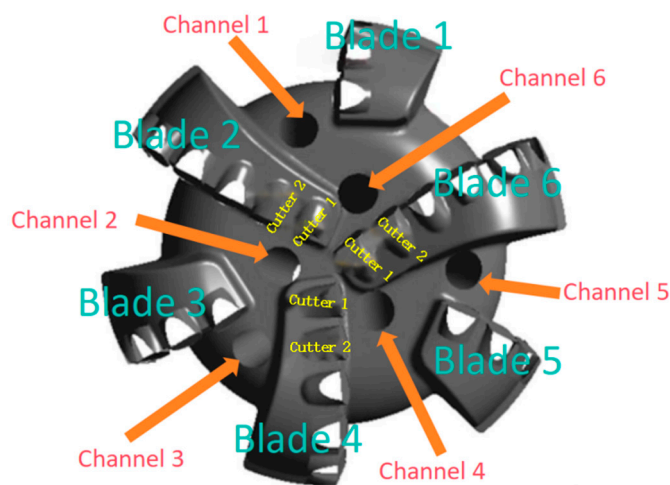


Figure 1. Three-dimensional model of six-blade PDC drill bit.

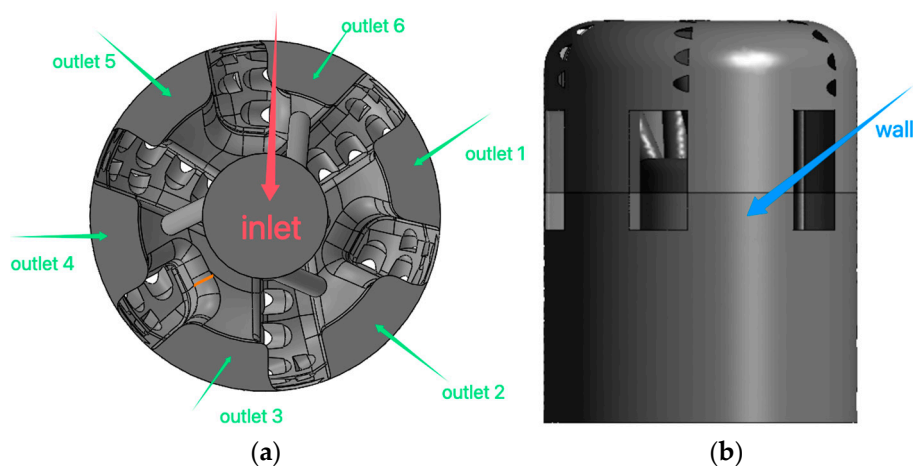


Figure 2. Schematic diagram of the model of the bottom hole flow calculation domain: (a) top view; (b) side view.

### 2.3.2. Mesh Generation

An unstructured tetrahedral mesh is used to discretize the bottom-hole flow of the PDC drill bit. Local mesh refinement is applied to critical regions, such as the cutters and nozzles, where detailed flow characteristics, such as velocity gradients and pressure distributions, must be accurately captured. In contrast, non-critical regions are meshed with a coarser grid to reduce computational costs while maintaining the overall accuracy of the simulation. A mesh independence analysis is performed to assess the effect of mesh density on the simulation results. Three mesh density schemes are designed for coarse, medium, and fine. The surface velocity variations of No. 1 cutter on No. 3 blade are used as the evaluation metric to compare the three schemes. As shown in Table 1, the velocity results from the medium mesh are within 0.59% of those from the fine mesh. The velocity changes significantly under the coarse mesh scheme, indicating insufficient mesh density. The medium mesh scheme is selected as the final mesh scheme to meet the balance between accuracy and computational efficiency, with the minimum mesh size set to 1.5 mm and the maximum mesh size set to 4 mm. The mesh of the bottom-hole flow domain is illustrated in Figure 3.

**Table 1.** Mesh-independent analysis.

Mesh Scheme	Minimum Mesh Size (mm)	PDC Cutter Velocity (m/s)
Coarse Mesh	3	9.012
Medium Mesh	1.5	9.567
Fine Mesh	1	9.624

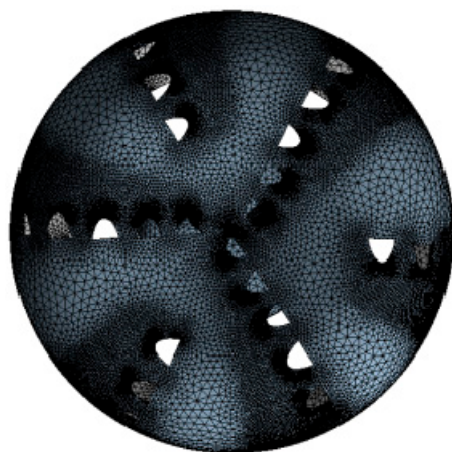


**Figure 3.** Mesh of the flow domain.

*2.4. Rock-Breaking Simulation Method*

This Section employs numerical modeling techniques and utilizes the Boolean operation functions of UG software (NX 12.0.0.27) to calculate the cutting volume of PDC cutters. The calculation of the cutting volume of the drill bit in the simulation essentially measures the volume of the removed material model [33]. Similarly, the material removal simulation method based on UG software involves simulating the actual motion of the tool and work-piece, using Boolean operations to remove material and ultimately obtaining the shape and relevant parameters of the model.

The first step involves extracting the curve edges of the PDC drill bit and identifying the arc-type edges while obtaining positioning parameters, such as midpoint coordinates, radius, and the normal vector of the plane in which the arcs lie. The parameters of arcs that are not part of the cutter surface and the duplicate parameters of arcs on the cutter surface are removed. The center coordinates of the arcs are sorted to determine the corresponding blade and PDC cutter numbers for each arc. Arcs are generated based on these valid positioning parameters, and the cutting trajectories for each cutter are established along a helical path. Boolean operations are performed between the cutting trajectories and a virtual rock layer to obtain the bottom-hole model during the drilling process. The contact surface of each cutter is formed at the intersection of the bottom-hole model and the endpoint circular surface of the cutting trajectory, representing the actual contact area between the cutter and the rock. Finally, using the analysis function in UG software, the contact area and arc length for each cutter are measured. The edge curves of the contact surface for each cutter are swept along its helical cutting trajectory to calculate the actual cutting volume for each cutter. After obtaining the cutting volume of each cutter, the cutting mass flow rate generated by each PDC cutter is calculated using Equation (10).

$$Q_s = \rho_s V_s \omega \tag{10}$$

where  $Q_s$  is the cuttings generation flow rate;  $\rho_s$  is the rock density;  $V_s$  is the cuttings volume after one cutting cycle;  $\omega$  is the drill bit speed.



All edge curves are extracted from the PDC drill bit model, and arc segments unrelated to the cutter surface are removed. Then, the center coordinates of the arcs related to the cutter surface and the distance from the center to the central axis of the bit are obtained. Based on the center coordinates of the arcs, the distance from the center to the central axis, and the rotation speed of the bit, the linear velocity of the PDC cutters is calculated, representing the initial motion velocity of the cuttings. The Equation is as follows:

$$U_s = C_s \omega \tag{11}$$

where  $U_s$  is the initial movement speed of the cuttings;  $C_s$  is the circumference of the cutters after one rotation.

The procedure for determining the initial motion direction of rock cuttings is as follows: The centers of all PDC cutters are projected onto the longitudinal plane, and these centers are connected to form a curve. This curve is then rotated around the bit axis to generate a surface. A line segment (L1) is drawn perpendicular to this surface at the center of each cutter. L1 is subsequently projected onto the cutter surface, creating a new line segment (L2). The coordinates of the endpoints of L2 are used to calculate a unit vector (E2), which represents the initial motion direction of the rock cuttings.

A rock-breaking simulation is conducted assuming a rotational speed of 120 r/min for the six-blade PDC drill bit and the cutting depth of the PDC cutter inserts of 3 mm. The simulation provides the initial mass flow rate, velocity, and motion direction of the rock cuttings for each cutter. Due to space constraints, only the parameters for the cutters on blade 1 are listed in Table 2, while Table 3 summarizes the total cutting volume for each blade.

**Table 2.** The rock cuttings parameters of blade No. 1.

Cutter Number	No. 1	No. 2	No. 3	No. 4	No. 5	No. 6	No. 7
mass flow rate (kg/s)	0.004	0.014	0.025	0.024	0.028	0.018	0.001
velocity (m/s)	0.107	0.35	0.592	0.851	1.096	1.249	1.281
direction (X)	0.016	0.005	0.038	−0.169	−0.609	−0.882	−0.902
direction (Y)	0.326	0.344	0.365	0.241	0.004	−0.149	−0.086
direction (Z)	−0.909	−0.901	−0.883	−0.904	−0.716	−0.287	0.002

**Table 3.** The initial cuttings mass flow rate of each blade.

Blade Number	No. 1	No. 2	No. 3	No. 4	No. 5	No. 6
Mass Flow Rate (kg/s)	0.114	0.069	0.101	0.081	0.108	0.071

### 2.5. Boundary Conditions

- Inlet conditions:** In this study, a viscous mud drilling fluid is used as the medium. The drilling fluid is characterized by a 1200 kg/m<sup>3</sup> density and a 0.02 Pa·s viscosity, which are typical values for water-based mud (WBM) commonly used in drilling operations. The inlet flow rate is set to 40 L/s to simulate the common flow conditions in the actual drilling process. The density of the rock cuttings is set to 2300 kg/m<sup>3</sup>, which is based on the physical properties of sandstone.
- Wall conditions:** The rotational speed of the drill bit is assumed to be 120 r/min. To simulate the rotation of the drill bit, the wall in the bottom-hole flow model is set to rotate at the same speed as the drill bit but in the opposite direction, thereby simulating the relative motion between the drill bit and the fluid.

3. Outlet conditions: The outlet is set as a pressure boundary with a pressure value of 18 MPa. This pressure is adjusted based on the actual well pressure data to ensure the accuracy and realism of the simulation results.
4. Initial conditions: The obtained cutting parameters (initial velocity, direction, and mass flow rate) are inserted into the corresponding PDC cutters as the initial conditions for numerical simulation.
5. A transient analysis of the bottom hole flow is performed to capture the dynamic changes in fluid and cuttings over time. The simulation duration is set to 5 s to ensure that the calculation has reached a steady state.

### 3. Results

#### 3.1. Bottom-Hole Flow Velocity Analysis

##### 1. Single-Phase Flow

As shown in Figure 4a, the bottom-hole flow velocity is relatively high, with no significant low-velocity areas observed, indicating that the drilling fluid effectively transports rock cuttings. In Figure 4b, two small vortices are visible in areas A and B, caused by the interference between the jet streams from the nozzles. The two vortices suggest that rock cuttings in areas A and B may not be efficiently transported, leading to gradual accumulation, which eventually results in bit-balling, negatively impacting drilling efficiency and operational safety. Therefore, it is essential to maintain a sufficiently high fluid velocity to enhance cutting transport and minimize or eliminate the formation of vortices, which helps prevent the accumulation of rock cuttings and mitigates associated drilling issues.

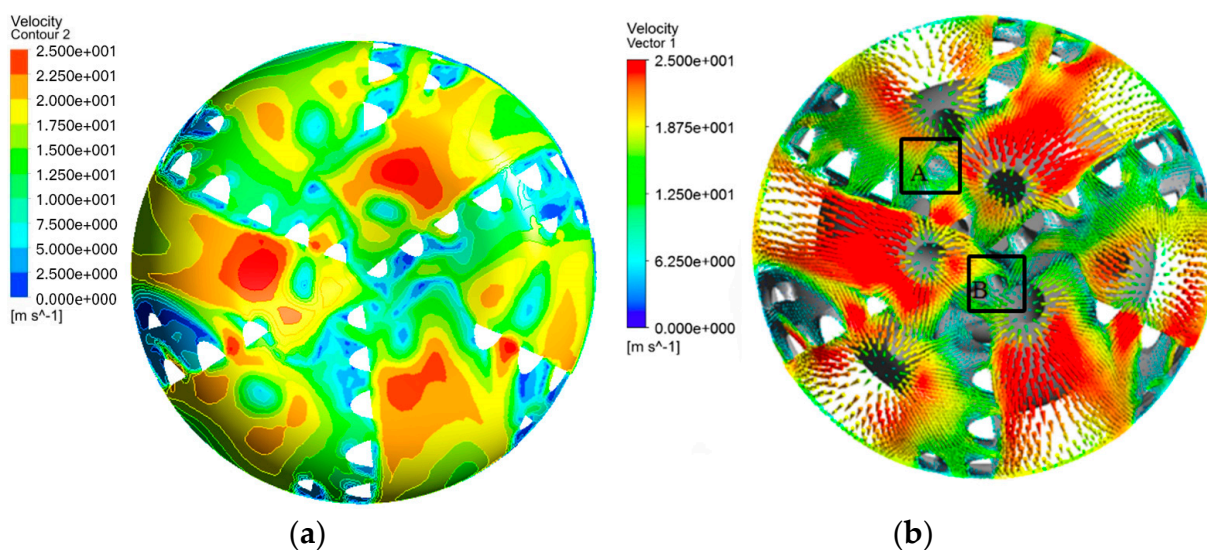
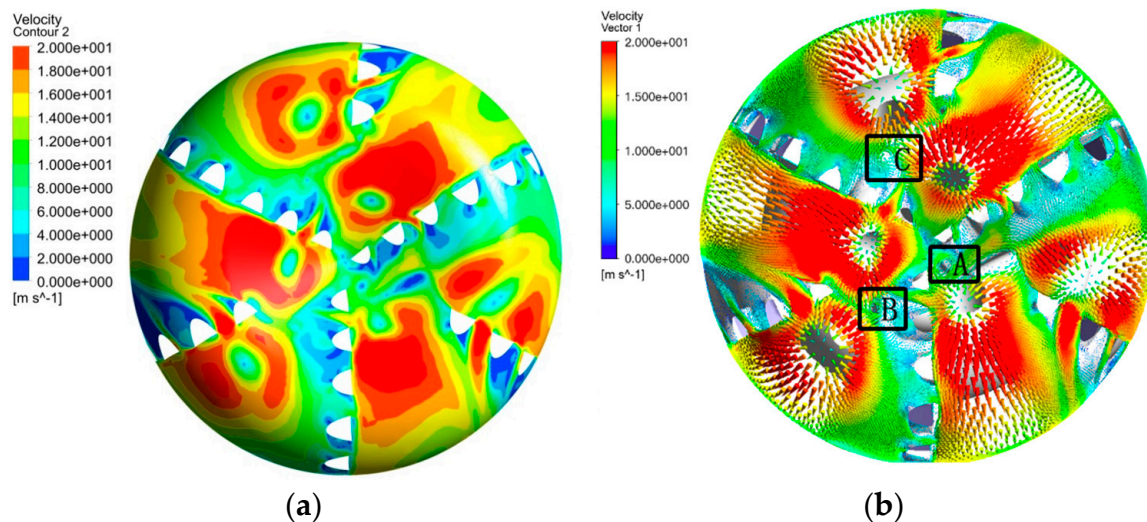


Figure 4. Bottom-hole flow velocity results: (a) velocity contour; (b) velocity vector cloud diagram.

##### 2. Two-Phase Flow

As illustrated in Figure 5a, the bottom-hole flow velocity in the liquid–solid two-phase flow is generally high. There is no significant low-flow velocity area at the center of the well bottom, indicating a relatively uniform velocity distribution. The highest flow velocity occurs near the nozzle. As shown in Figure 5b, vortices are also observed in the liquid–solid two-phase flow at areas A, B, and C. The three vortices indicate that rock cuttings may not be efficiently transported away and could accumulate at these regions, potentially reducing drilling efficiency.



**Figure 5.** Bottom-hole flow velocity results: (a) velocity contour; (b) velocity vector cloud diagram.

### 3.2. Analysis of Cutter Cleaning and Cooling Efficiency

#### 1. Single-Phase Flow

Figures 6–8 illustrate the surface velocity distribution of primary blades No. 1, No. 3, and No. 5. The results show that the fluid velocity on the main cutters of all primary blades is relatively low, particularly No. 4 and No. 5 cutters of each blade. The low fluid velocity on the main cutters suggests insufficient hydraulic energy, which may hinder the cleaning and cooling of the cutter surface. The main PDC cutters perform the primary rock-breaking function during drilling, generating substantial rock cuttings. Therefore, a higher fluid velocity is required to ensure the timely removal of these rock cuttings from the main PDC cutters. Conversely, No. 1, No. 2, and No. 7 cutters, which produce fewer rock cuttings, have higher flow velocities, indicating a waste of hydraulic energy. The low fluid velocity on the main cutters and the high velocity on the other cutters result in an uneven hydraulic energy distribution across the drill bit, which could compromise the cleaning and cooling of the cutter surface, ultimately reducing drilling performance. Therefore, optimizing the hydraulic structure design for these three primary blades is essential.

#### 2. Two-Phase Flow

Two key metrics were introduced to comprehensively assess the cleaning and cooling efficiency of drilling fluid on cutters: surface velocity percentage ( $V$ ) and cutting mass percentage ( $M$ ). The surface velocity percentage ( $V$ ) represents the percentage of the surface flow velocity on each PDC cutter relative to the nozzle outlet flow velocity, while the cutting mass percentage ( $M$ ) indicates the percentage of the cuttings mass flow rate generated by each PDC cutter relative to the total cuttings mass flow rate of the blade where the cutter is located.

The two curves of  $V$  and  $M$  were plotted for each blade. According to the hydraulic energy distribution principle, the evaluation criteria for the hydraulic structure are as follows: PDC cutters that generate more rock cuttings require higher drilling fluid velocities, while those producing fewer rock cuttings need lower fluid velocities. Ideally, the distribution trends in the two curves should align, indicating a balanced hydraulic energy distribution across the blade.

Figure 9 shows that the trend distribution of surface velocity and cutting mass percentage varies significantly among the cutters. Specifically, No. 4, No. 5, and No. 6 cutters exhibit higher cutting mass flow rates and display the lowest surface flow velocities, which may adversely affect the cleaning and cooling efficiency of the three cutters, resulting in

the accumulation of rock cuttings and increase thermal wear, ultimately reducing drilling performance. Conversely, No. 1 and No. 7 cutters, which generate the lowest cutting mass flow rates, exhibit disproportionately high surface flow velocities, indicating inefficient use of hydraulic energy. Optimizing the hydraulic structure by refining the injection angle and placement of the nozzle could promote a more balanced distribution of hydraulic energy.

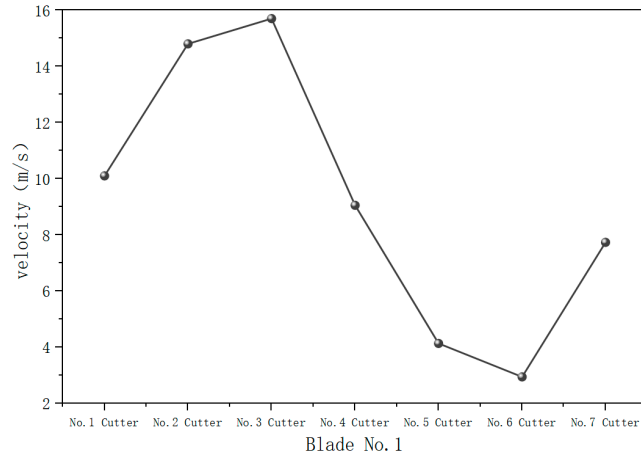


Figure 6. Surface velocity of blade No. 1.

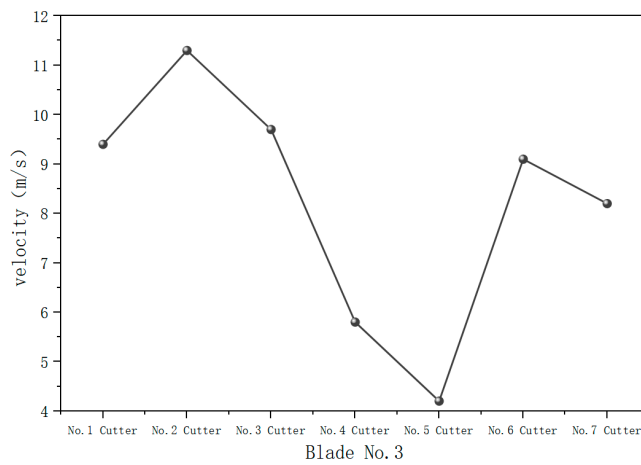


Figure 7. Surface velocity of blade No. 3.

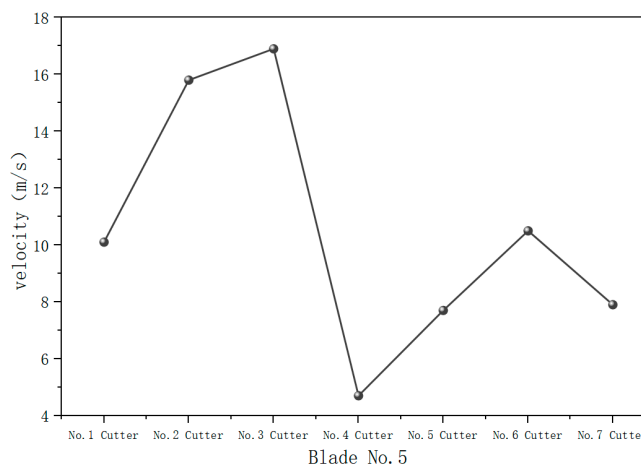
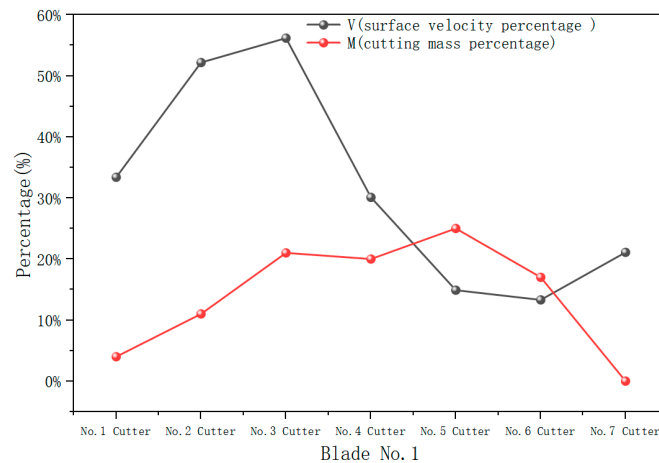
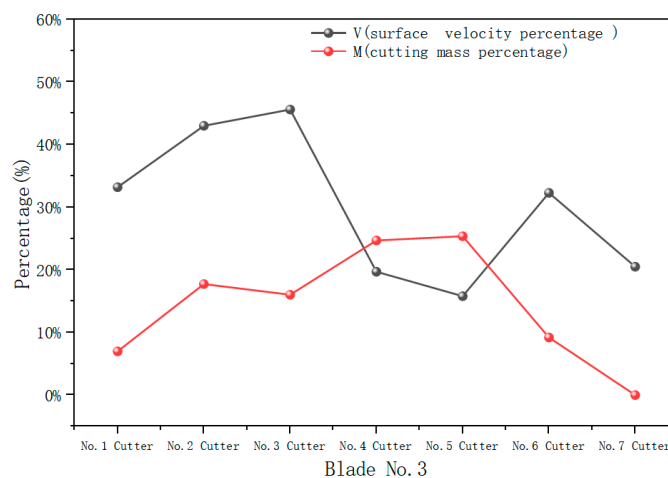


Figure 8. Surface velocity of blade No. 5.



**Figure 9.** Surface velocity distribution of blade No. 1.

As shown in Figure 10, the surface velocity curve of the cutters on blade No. 3 differs significantly from the cutting mass distribution curve. No. 4 and No. 5 cutters have the highest cutting mass flow rates and exhibit the lowest fluid velocities. Such low fluid velocity may affect the cleaning and cooling efficiency of the cutter surfaces, potentially leading to bit balling and thermal wear, thereby reducing drilling efficiency and increasing costs. Conversely, No. 6 and No. 7 cutters, with the lowest cutting mass flow rates, show relatively high surface velocities, indicating that the hydraulic structure of blade No. 3 requires further optimization, which can be achieved by adjusting the angle of the nozzle to achieve a more balanced hydraulic energy distribution.



**Figure 10.** Surface velocity distribution of blade No. 3.

As shown in Figure 11, the surface velocity curve of blade No. 5 is concave, which is obviously different from the trend in the cutting mass curve. The surface velocity of No. 4 cutter with the highest cutting mass flow rate is the lowest, while the surface velocity of No. 1, No. 6, and No. 7 cutters with the lowest cutting mass flow rate is higher, resulting in a waste of hydraulic energy. Therefore, it is necessary to adjust the nozzle angle to optimize the hydraulic structure and achieve a reasonable distribution of hydraulic energy.

As shown in Figure 12, the surface velocity curve of No. 6 blade is generally flat, with no significant fluctuations, which differs from the distribution of the cutting mass percentage curve. Specifically, the surface velocities of No. 4 and No. 5 cutters, which have the lowest cutting mass flow rates, are higher, potentially leading to a waste of hydraulic energy. In contrast, the surface velocity of No. 2 cutter, which has the highest cutting mass flow rate, is lower. Although the surface velocity of No. 2 cutter remains sufficiently high



to ensure effective cleaning and cooling, it does not align with the principle that higher cutting mass flow rates should correspond to higher surface velocities, and lower cutting mass flow rates should correspond to lower velocities. Therefore, further optimization of the hydraulic structure design is necessary to ensure the efficient and scientific distribution of hydraulic energy.

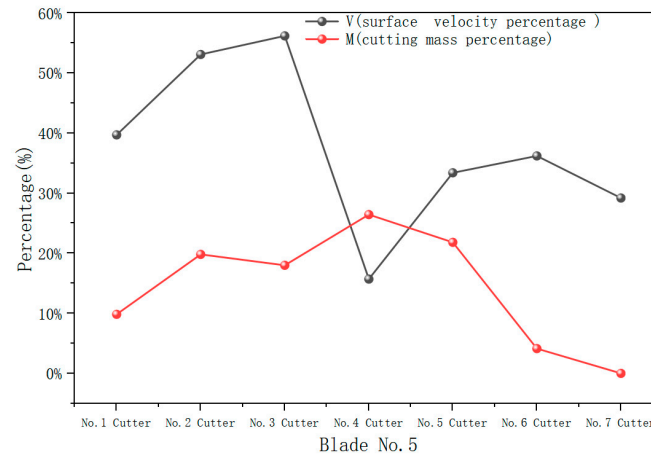


Figure 11. Surface velocity distribution of blade No. 5.

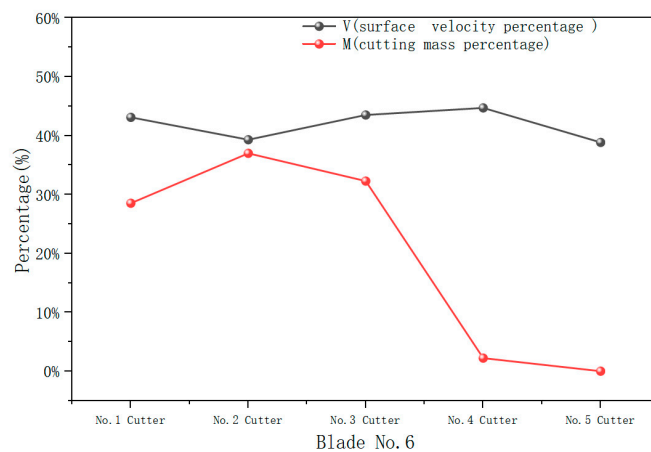


Figure 12. Surface velocity distribution of blade No. 6.

### 3.3. Analysis of Drill Bit Body Erosion

The numerical simulation of the liquid–solid two-phase flow not only provides information about the flow of fluids and rock cuttings around the drill bit but also allow for assessing the erosion on the drill bit surface. Drilling fluid is required to ensure the cleaning and cooling effect of the drill bit while avoiding excessive hydraulic energy that could lead to erosion. During the drilling process, the drilling fluid is sprayed at high speed onto the well bottom, carrying a large number of rock cuttings of varying sizes, forming a complex multiphase flow. During the circulation of the drilling fluid, the rock cuttings come into contact with the PDC drill bit, leading to wear and erosion. According to the Finnie erosion model, the erosion rate is calculated based on the interaction between the drill bit and the rock cuttings in the drilling fluid, typically related to the impact velocity of the rock cuttings and the hardness of the metal surface. The model accumulates the erosion rate over time, quantifying the cumulative erosion effect, which results in the erosion density. The total erosion rate cloud map of the drill bit surface is obtained through CFD post-processing.

As shown in Figures 13–15, the drill bit erosion is significantly different on different blades and cutters. The results are as follows:

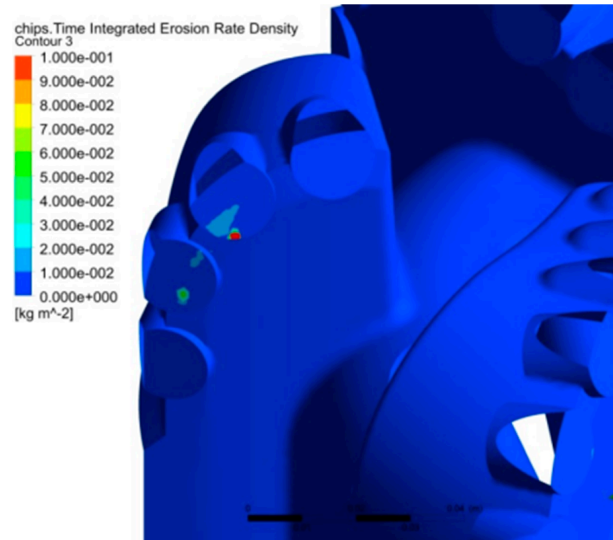


Figure 13. Erosion rate of blade No. 2.

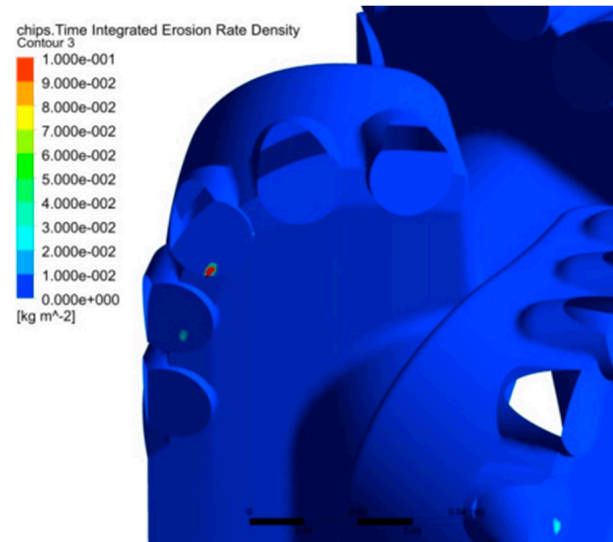


Figure 14. Erosion rate of blade No. 4.

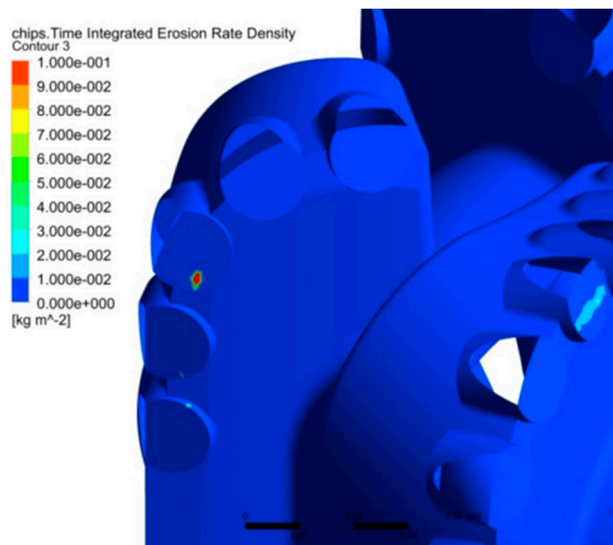


Figure 15. Erosion rate of blade No. 6.

During drilling, PDC cutters gradually wear due to continuous friction with the rock and the high-speed scouring effect of the drilling fluid. Numerical simulation results reveal significant erosion on the surfaces of No. 2 cutter (blade No. 2), No. 3 cutter (blade No. 4), and No. 3 cutter (blade No. 6). The erosion primarily concentrates on the surfaces and roots of the cutters, potentially leading to localized damage. Once erosion pits form, the local fluid velocity and turbulence intensity increase markedly. This results in a higher frequency of rock cuttings impacts, further aggravating surface and root erosion, which may cause PDC cutters to fall off or break. By contrast, no severe erosion is observed on the other blades, making further discussion unnecessary.

Erosion shortens the lifespan of PDC cutters and compromises the overall performance of the drill bit. The metal spalling caused by erosion may block downhole equipment, exacerbate wear on other components, and increase operational risks during drilling. Optimizing hydraulic structure design by adjusting nozzle angles and positions is recommended to minimize fluid energy in areas of high localized erosion. Additionally, improving the material properties of the PDC drill bit, such as utilizing more erosion-resistant alloys or applying advanced surface coatings, can help extend the lifespan of the drill bit, enhance drilling efficiency, and lower drilling costs.

#### 4. Discussion

This paper uses numerical simulation analysis to compare the flow characteristics of PDC drill bits under single-phase flow and liquid–solid two-phase flow. The results indicate that the velocity distribution at the bottom-hole exhibits a high degree of consistency under both conditions, with the highest velocity observed near the nozzles, gradually decreasing outward. The observed velocity distribution is due to the high-speed ejection of drilling fluid through the nozzle; the lateral flow generated after the jet impacts the bottom-hole primarily drives rock cuttings transportation and bit cooling, consistent with the findings of Hou Cheng et al. [14,15], who concluded that the lateral flow generated by the nozzle jet is the primary driving force for rock removal, with its velocity distribution decreasing from the center to the periphery. The rock-carrying capacity of the jet can be inferred by analyzing the velocity contour at the bottom-hole, which indirectly confirms the reliability of the liquid–solid two-phase flow simulation. In single-phase flow simulation, only two vortex areas are observed at the bottom-hole. The liquid–solid two-phase flow simulation reveals three distinct vortex areas (A, B, and C in Figure 5). Different simulation results show that rock cuttings produce complex dynamic effects. The rock cuttings alter the viscosity and density distribution of the fluid, causing local flow instabilities, which expand the vortex areas and change the vortex distribution. The vortex positions in the liquid–solid two-phase flow are similar to those in the single-phase flow, indicating that the bottom-hole geometry and flow conditions still dominate the main flow characteristics. However, introducing rock cuttings complicates the vortex formation mechanism, involving factors such as particle distribution, particle–liquid interactions, and boundary layer disturbances caused by the rock cuttings. As a result, the liquid–solid two-phase flow simulation can provide a more comprehensive and detailed view of the bottom-hole flow, offering more explicit flow distribution information than the single-phase flow simulation.

Single-phase flow analysis indicates that the surface flow velocities around the main cutters of No. 1, No. 3, and No. 5 blades are relatively low, suggesting potential deficiencies in the ability of fluid to clean and cool these main cutters adequately. However, the single-phase model does not account for the presence and impact of rock cuttings, leading to a less comprehensive evaluation of the hydraulic performance. In contrast, the liquid–solid two-phase flow analysis provides a more detailed and accurate assessment of the performance of each cutter. The model reveals that certain cutters, such as No. 4, No. 5, and No. 6 cutters on

No. 1 blade and cutter No. 4 on No. 5 blade, exhibit low surface flow velocities, which may hinder effective cleaning and cooling, leading to issues like bit-balling, increased friction, and potential overheating, ultimately impairing drilling performance. Conversely, cutters with lower cutting mass flow rates, such as No. 1 and No. 7 cutters on No. 1 blade, show higher surface velocities, potentially leading to unnecessary hydraulic energy expenditure. By incorporating the effect of rock cuttings, the liquid–solid two-phase flow model offers a more precise evaluation than single-phase flow models and provides actionable insights for optimizing the hydraulic structure. This approach contrasts with previous research that often relied on qualitative analyses of surface flow velocity without fully considering the impact of rock cuttings, which may lead to incomplete or inaccurate conclusions [34,35].

The analysis reveals that significant surface erosion occurs on specific cutters, notably No. 2 cutter on No. 2 blade, No. 3 cutter on No. 4 blade, and No. 3 cutter on No. 6 blade. The erosion in these areas is likely due to the combined effects of high hydraulic energy and uneven jet impact pressure. As the high-velocity drilling fluid exits the nozzle, it transports rock cuttings of various sizes to the well bottom, where uneven impact pressure can cause rock cuttings to reverse and create a turbulent multiphase flow. Unlike single-phase flow analysis, which cannot fully account for the presence and impact of rock cuttings, liquid–solid two-phase flow simulations provide a more accurate representation of erosion patterns. Compared with existing literature, which mainly relies on single-phase flow simulations to indirectly analyze drill bit erosion based on surface velocity [12,36], liquid–solid two-phase flow simulations offer a higher accuracy. By directly capturing erosion damage, the results from liquid–solid two-phase flow simulations offer crucial insights into drill bit performance and design that surpass the predictive capabilities of traditional single-phase simulations.

When utilizing CFD post-processing simulation software for analysis, it is crucial to carefully assess the reliability and inherent limitations of the resulting data. CFD simulations depend heavily on the accuracy of the underlying physical models and numerical methods, which are often built upon simplifications such as assuming uniform particle distribution or neglecting finer turbulence scales. These simplifications can introduce discrepancies between the simulation outcomes and real-world conditions. Furthermore, the precise definition of boundary and initial conditions plays a pivotal role in shaping the accuracy. However, these conditions often fail to capture the full complexity of actual operational environments. Additionally, ANSYS-CFX version 2022.R1 may encounter limitations when addressing intricate flow phenomena, such as vortex formation or high-velocity erosion, where its predictive capabilities might need to be improved. Consequently, while CFD provides a robust framework for analysis, its results should be validated against experimental data to ensure reliability. It is also essential to account for potential inaccuracies stemming from the assumptions and simplifications inherent in the model.

## 5. Conclusions

Based on a comprehensive analysis of the current research status and existing issues regarding numerical simulations of the bottom-hole flow for PDC drill bits, this paper establishes a numerical simulation technique for liquid–solid two-phase flow in the rotational flow of PDC drill bits, grounded in the basic theory of CFD and multiphase flow. By integrating CFD with rock-breaking simulation methods, the parameters of the rock cuttings generated on the surfaces of PDC cutters are obtained and used as boundary conditions for the two-phase flow calculation model. The developed liquid–solid two-phase flow simulation reflects actual drilling conditions more accurately, further improving the numerical simulation techniques for liquid–solid two-phase flow around PDC drill bits. Compared to existing literature, previous studies have established liquid–solid two-phase

flow simulation methods but often overlooked the initial generation location of the rock cuttings, assuming the rock cuttings are generated directly from the bottom-hole, which does not align with actual drilling conditions. The study contrasts single-phase and two-phase flow simulations, revealing that the latter uncovers more design issues in the hydraulic structure of the drill bit. The results from the two-phase flow simulation offer a more detailed view of the hydraulic performance and effectively guide design improvements to enhance the efficiency and longevity of the bit.

## 6. Future Work Recommendations

This paper also has certain limitations. Firstly, the lack of experimental validation is an issue. Although a liquid–solid two-phase flow model for the bottom-hole flow of PDC drill bits has been established through numerical simulations, the absence of actual experimental data for comparison and validation may affect the reliability and accuracy of the predictive results. Secondly, the method established in this paper is only applicable to simulations of the bottom-hole flow of PDC drill bits under conditions without solid particles in the drilling fluid. In drilling operations involving drilling fluids containing solid particles, the fluid interacts with these particles and rock cuttings, forming a liquid–solid–solid three-phase flow mixed at the bottom hole. Similarly, in gas drilling, gas and cuttings form a gas–solid two-phase flow. Researching the multiphase flow at the bottom hole in different drilling operations is essential for improving bottom-hole flow distribution and enhancing drill performance. Future research will need to validate the effectiveness of the model through experiments and further investigate its applicability under more complex bottom-hole conditions.

Additionally, this study uses the  $k-\varepsilon$  model and wall function model for turbulence simulations, which have limitations in capturing complex flow conditions. The  $k-\varepsilon$  model often requires wall functions to improve accuracy near walls but can still struggle with high strain rate flows. The  $k-\omega$  model provides better accuracy in near-wall regions without additional wall functions but may not perform as well in free-shear flows. Future research should consider incorporating the  $k-\omega$  model to enhance the accuracy and adapt to different flow conditions.

**Author Contributions:** L.W.: conceptualization, methodology, validation, writing—original draft, writing—review and editing, conceptualization; J.H.: funding acquisition, supervision, writing—review and editing. All authors have read and agreed to the published version of the manuscript.

**Funding:** This research received funding from Mapua University.

**Data Availability Statement:** The original contributions presented in the study are included in the article, further inquiries can be directed to the corresponding author.

**Conflicts of Interest:** The authors declare no conflicts of interest.

## References

1. Deng, R.; Li, Y. Simulation analysis of temperature field for PDC bit cutter rock breaking. *China Pet. Mach.* **2012**, *40*, 37–42.
2. Guan, Z.; Chen, T.; Liu, X. Review of Studies of PDC Bit Hydraulic Configurations. *J. Univ. Pet.* **1994**, *16*, 136–142.
3. Chen, X.; Zou, D. Bit Balling Mechanism and Research Progress in Countermeasures for PDC Bit Drilling in Mud Shale Formations. *Nat. Gas Ind.* **2014**, *34*, 87–91.
4. He, L.; Xie, C.; Kang, M. Numerical Simulation About Effect of Flow Path on PDC Bit Fluid Field. *J. Univ. Shanghai Sci. Technol.* **2007**, *29*, 59–64.
5. Tang, D.; Luo, C.; Deng, Z. Design of the Gear Hydraulic Motor of the Rotary Shaft Core Drill Bit. *J. Mach. Des.* **2007**, *43*, 119–124.
6. Hua, T. Numerical Simulation of DTH Bits Gas-Solid Two-Phase Flow in Air Drilling. *J. Cent. South Univ.* **2011**, *42*, 3040–3047.
7. Xie, C.; Yang, A.; Wang, H.; Chen, K. Numerical Research on Emerged Multi-Stream Jetting at Limited Bottom-Hole Space of Drill Bits. *Fluid Mach.* **2002**, *30*, 25–27.



8. Xie, C. Numerical Simulation for Downhole Flow Field of Jet on PDC Bits with Asymmetric Multi-Nozzle Distribution. *Acta Pet. Sin.* **2002**, *23*, 77–80.
9. Huang, H.; Zhai, Y. Numerical Simulation and Experimental Checking for Downhole Flow Field of a Real PDC Bit. *J. Univ. Pet. China Nat. Sci. Ed.* **2005**, *29*, 49–52.
10. Gang, B.; Li, M.; Dou, L.; Qu, Z. Research on Structure Design and Flow Field Characteristics of the Novel Jet Bit for Radial Horizontal Drilling. *Energy Sci. Eng.* **2018**, *6*, 535–547.
11. Saifulizan, S.S.B.H.; Busahmin, B.; Elmabrouk, S. Evaluation of Different Well Control Methods Concentrating on the Application of Conventional Drilling Technique. *ARPN J. Eng. Appl. Sci.* **2023**, *18*, 1851–1857.
12. Peng, W.; Cao, X. Numerical simulation of solid particle erosion in pipe bends for liquid-solid flow. *Powder Technol.* **2016**, *294*, 266–279. [[CrossRef](#)]
13. Guo, R.; Li, G.; Huang, Z.; Tian, S.; Shi, H. Numerical Simulation Study on Flow Field of Multi-Hole Jet Bit. *Fluid Mach.* **2010**, *38*, 13–17.
14. Hou, C.; Li, G.; Huang, Z.; Tian, S.; Shi, H. Research on Characteristics of Bottomhole Flow Field of PDC Bit with Side Nozzles. *Pet. Drill. Tech.* **2010**, *32*, 15–18.
15. Chen, X.; Zou, D. Optimization of Hydraulic Parameters for PDC Bits Based on Minimization of Mud Packing. *Spec. Oil Gas Reserv.* **2014**, *21*, 142–144.
16. Xu, J. Design and Application of New Anti-balling PDC Bit for Shale. *Pet. Mach.* **2014**, *42*, 12–15.
17. Yu, J. On Measures for Treating PDC Bit Bailing and New Type of Bits against Bailing-Up. *J. Jiangnan Pet. Univ.* **2013**, *26*, 46–48.
18. Rahman, M.R.A.; Busahmin, B.; Hasan, U.H.H. Analysis of a drilling mud-based system on the common problems related to coiled tubing application in slim-hole oil wells. *Edelweiss Appl. Sci. Technol.* **2023**, *7*, 71–86. [[CrossRef](#)]
19. Huang, K.; Feng, Y.; Zhou, C.; Chen, L.; Yang, Y.; Wang, X.; Fu, C. Analysis of Bit-Balling Failure and Hydraulic Structure Optimization Design of Annular-Grooved PDC Bits. *Geoenergy Sci. Eng.* **2024**, *241*, 213134. [[CrossRef](#)]
20. Qu, P.; Dan, B.; Chen, G.; Niu, Q.; Ye, D.; Zhang, X. Influence of PDC Bit Design Parameters on Bottomhole Flow Field Distribution. *Mach. Tool Hydraul.* **2023**, *13*, 160–165.
21. Wang, Y.; Zhang, S.; Wang, W.; Lue, L. CFD Numerical Simulation Analysis of PDC Bits in Rotating Flow Field. *Yunnan Chem. Ind.* **2019**, *46*, 174–175.
22. Wu, Z.; Wang, Y.; Pan, Y.; Wang, W.; Lue, L. Comparative Study on Simulation of Rotating Flow Field and Non-Rotating Flow Field of PDC Bit. *Oilfield Mach.* **2020**, *49*, 10–15.
23. Feng, C.; Liu, W.; Gao, D. CFD Simulation and Optimization of Slurry Erosion of PDC Bits. *Powder Technol.* **2022**, *408*, 117658. [[CrossRef](#)]
24. Zhao, J.; Zhang, G.; Xu, Y.; Wang, R.; Zhou, W.; Yang, D. Experimental and Theoretical Evaluation of Solid Particle Erosion in an Internal Flow Passage Within a Drilling Bit. *J. Pet. Sci. Eng.* **2018**, *160*, 582–596. [[CrossRef](#)]
25. Zhao, J.; Zhang, G.; Xu, Y.; Wang, R.; Zhou, W.; Han, L. Bit Internal Flow Passage Erosion by Solid-Liquid Two-Phase Flow Impact of Particles. *J. Cent. South Univ.* **2018**, *49*, 1228–1236.
26. Chen, Z.; Wang, M.; Li, X.; Shi, H.; Fan, Y.; He, W. Numerical Simulation Study and Field Test of Bottom-Hole Flow Field of PDC Bits. *Drill. Eng.* **2023**, *46*, 85–93.
27. Cao, L.; Zhang, H.; Wang, W.; Yan, J.; Hu, C. CFD Simulation Study of Two-Phase Flow Field in Enclosed Coring Bit. *Drill. Eng.* **2021**, *11*, 35–41.
28. Li, J.; Bian, C.; Liu, Z. Study on Flow Field Characteristics of Rotary Cutting PDC Bit Based on DPM Model. *Pet. Mach.* **2021**, *49*, 24–32.
29. Pu, G. *ANSYS Workbench Basic Tutorials and Detailed Examples*, 2nd ed.; China Water Conservancy and Hydropower Press: Shanghai, China, 2013; pp. 48–56.
30. Wang, F. *Principles and Applications of CFD Software for Computational Fluid Dynamics Analysis*; Tsinghua University Press: Beijing, China, 2004; pp. 5–8.
31. Kalitzin, G.; Medic, G.; Iaccarino, G.; Durbin, P. Near-wall behavior of RANS turbulence models and implications for wall functions. *J. Comput. Phys.* **2005**, *204*, 265–291. [[CrossRef](#)]
32. Burns, A.D.; Frank, T.; Hamill, I. The favre averaged drag model for turbulent dispersion in Eulerian multi-phase flows. *J. Fluid Mech.* **2004**, *392*, 67–93.
33. Liao, Z.; Wu, Z.; Wei, Q. Calculating the cutting parameters of PDC BIT with Pro/TOOLKIT. *Pet. Mach.* **2005**, *34*, 47–50.
34. Li, W.; Yang, H.; Liu, S. Characteristics Simulation of Rotary Nozzle Flow Field of PDC Bits. *Oilfield Mach.* **2023**, *52*, 26–32.
35. Tan, C.; Wang, W.; Li, W. Numerical Simulation and Optimization of Bottomhole Flow Field in a New PDC Bit. *Drill. Prod. Technol.* **2022**, *45*, 31–35.
36. Liu, X. *Numerical Simulation of Erosion Wear in Spiral Axial Flow Mixed Transportation Pump Inlet Pipeline*; China University of Petroleum: Beijing, China, 2018.

**Disclaimer/Publisher’s Note:** The statements, opinions and data contained in all publications are solely those of the individual author(s) and contributor(s) and not of MDPI and/or the editor(s). MDPI and/or the editor(s) disclaim responsibility for any injury to people or property resulting from any ideas, methods, instructions or products referred to in the content.